PIER C

(Received 1 October 2025, Accepted 10 December 2025, Scheduled 20 January 2026)

Corporate-Fed Inclined Patch Arrays for Meteorological Direct Broadcast Reception

Paramasivam Jothilakshmi[1,*] and Rajendran Mohanasundaram[2]

[1]*Department of Electronics and Communication Engineering*
Amrita School of Engineering, Amrita Vishwa Vidyapeetham, Chennai, India
[2]*Department of Electronics and Communication Engineering*
Sri Venkateswaraa College of Technology, Chennai, India

ABSTRACT: This work codesigns and validates a compact microstrip patch array with a corporate feed for meteorological direct broadcast at 7.5 GHz, comparing 1×4 to 1×64 arrays. Square patches with rounded corners are rotated 45° to suppress modes, reduce coupling, and preserve broadside radiation. The feed network delivers equal amplitude to four ports. A neural network surrogate trained on full-wave samples accelerates the exploration of edge length, corner radius, spacing, rotation, and feed-line dimensions while enforcing limits on S_{11} and coupling. The 1×4 prototype utilizes Rogers RT Duroid 5880, $\varepsilon_r = 2.2$, thickness 0.787 mm, with a substrate size of 120 mm × 75 mm. Photolithography and anechoic measurements confirm a 7.5 GHz center frequency, broadside radiation, peak gain above 14 dBi, and a 450 MHz bandwidth. Scaling to 1×64 shows 3 dB gain per doubling, reduced beamwidth, stable bandwidth, and coupling; sensitivity studies verify robustness.

1. INTRODUCTION

Microstrip linear array antennas are central to X-band satellite terminals because of low mass, planar integration, and straightforward fabrication [1, 2]. Prior studies have shown how patch geometry, feed topology, substrate choice, and inter-element coupling shape performance in the 7 to 8 GHz regime [3, 4]. Uniform broadside excitation yields high directivity but elevated sidelobes [5], which motivates classical tapers such as Dolph Chebyshev and Taylor to balance main beam sharpness and sidelobe suppression [6, 7]. Element investigations on square, rectangular, and circular patches pursue wider bandwidth, polarization control, and simpler manufacture [8]. Low-loss dielectrics such as Rogers RT Duroid 5880 provide stable permittivity and low dissipation, enabling repeatable resonances and improved efficiency [9, 10]. Two constraints persist for compact meteorological direct broadcast ground terminals. Dense spacing intensifies mutual coupling, degrading impedance and radiation patterns [11, 12], and exhaustive full-wave optimization across coupled geometric and feed parameters becomes prohibitive as apertures grow [13, 14]. Conventional mitigations, including defected grounds, electromagnetic band gaps, and parasitic inclusions, can help but often add layout complexity or height [15, 16]. Inclined patch arrays reduce coupling by rotating neighboring elements, disrupting dominant surface wave paths while retaining broadside radiation [17, 18]. Together with a well-matched corporate feed beneath the radiators, the architecture preserves equal amplitude and phase from a single radio frequency (RF) input without excessive routing overhead [19, 20], although selecting inclination, spacing, perturbations, and feed dimensions remains a coupled and high-dimensional task [21, 22].

This work targets 7.5 GHz meteorological direct broadcast using a surrogate accelerated codesign that treats radiators and corporate feed as one optimization object. A data-driven model trained on full-wave samples surveys patch edge length and corner radius, element rotation, spacing, and feed widths and offsets under constraints on return loss, inter-element coupling, and amplitude and phase balance [23–25]. The methodology validates a compact 1×4 array on RT Duroid 5880 and then scales the workflow to 1×8, 1×16, 1×32, and 1×64 apertures for consistent comparison. Results quantify gain, half-power beamwidth, sidelobe level, and impedance bandwidth. Gain approaches the expected 3 dB per doubling; beamwidth narrows with array length; bandwidth remains near the design target; and coupling is moderated by inclination and spacing rules. Sensitivity analyses spanning etch tolerances and modest permittivity shifts confirm robustness. Contributions are threefold: an experimentally verified integrated radiator plus feed codesign for inclined arrays at 7.5 GHz, a surrogate that expedites multi-objective exploration while enforcing practical constraints, and a unified scaling study from 1×4 to 1×64 that guides low-profile high-gain X-band arrays for compact ground terminals in meteorological direct broadcast reception.

2. DESIGN AND EVOLUTION OF INCLINED LINEAR ARRAY ANTENNA

The development shown in Figure 1 begins with a square microstrip patch, which is easy to design and fabricate; however, it exhibits a narrow bandwidth and high surface current at sharp

* Corresponding author: Paramasivam Jothilakshmi (jothivishnu1212@gmail.com).

TABLE 1. Performance summary (Predicted): 1×4 inclined microstrip patch array using ANN model.

Angle (°)	Return Loss (dB)	Gain (dBi)	Directivity (dBi)	Efficiency (%)	Sidelobe level (dB)	Bandwidth (%, −10 dB)	Bandwidth (GHz)
5	−15.38	8.08	8.94	64.50	−10.84	3.45	0.39
10	−15.83	9.13	9.96	69.00	−11.80	3.88	0.43
15	−16.75	10.15	10.93	73.50	−12.96	4.30	0.48
20	−18.33	11.12	11.86	78.00	−14.29	4.69	0.53
25	−20.50	12.05	12.77	82.50	−15.67	5.06	0.57
30	−22.63	12.97	13.70	87.00	−16.96	5.41	0.61
35	−23.90	13.90	14.67	91.50	−18.08	5.76	0.65
40	−24.74	14.86	15.68	93.00	−19.02	6.12	0.69
45	−25.55	15.86	16.72	95.00	−19.84	6.50	0.73

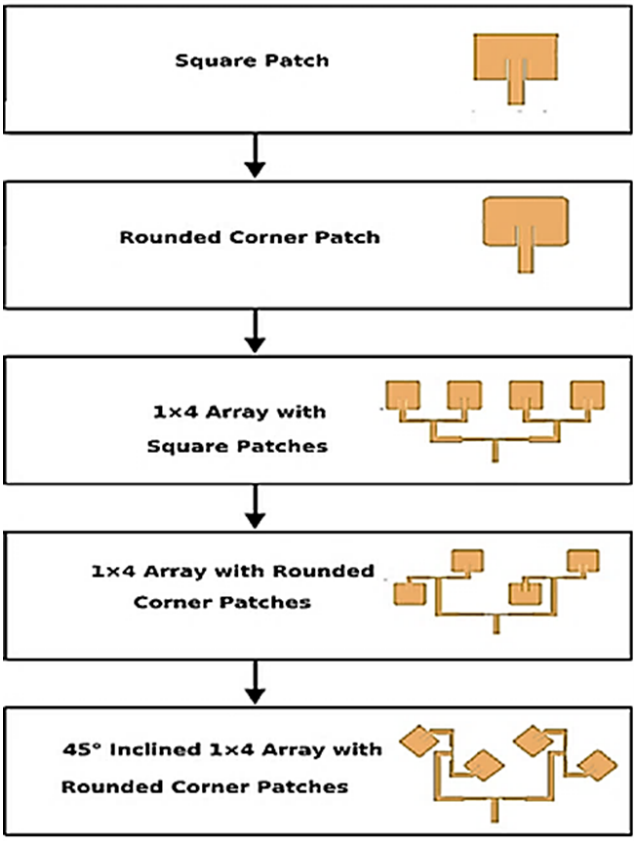

FIGURE 1. Evolution of 45° inclined 1×4 LAA with a rounded corner square patch.

corners. The design evolves to a 1×4 rounded square array for X-band. Rounding each corner alleviates current crowding, broadens bandwidth, and smooths the pattern. Four patches are fed by a corporate divider with a 50 Ω input that splits into two 100 Ω branches and then into two matched feeds. Equal path lengths preserve the phase. Rotating each patch by 45° improves polarization purity and reduces sidelobes, yielding a compact, matched array. The proposed microstrip patch antenna is designed using the standard design equation [26, 27].

Figure 2 compares five configurations at 7.5 GHz: a square patch, a rounded corner patch, a 1×4 array from the square geometry, a rounded corner array, and a 45° inclined rounded corner array. Return loss improves from −18 dB for the square element to nearly −26 dB for the inclined array. The transition from a rounded single patch to the 1×4 array yields −22.8 dB with better matching. Gain rises from 7.5 to 15 dBi, and directivity increases from 8.5 to 16.7 dBi, confirming stronger beam focusing. Radiation efficiency grows from 80% to 95%. Sidelobe level falls from −10 to −19 dB. Bandwidth at 7.5 GHz nearly doubles, from 0.225 to 0.45 GHz, giving the best overall balance. Pattern purity also improves. In a microstrip line, the electromagnetic fields are present in both the dielectric substrate and the air above it, resulting in wave propagation as if in a medium with a permittivity that is intermediate between that of the substrate (ε_r) and free space.

The optimization workflow defines objectives, fabrication limits, and geometric parameters for the sloped microstrip array. Latin hypercube sampling is used to generate the initial design set for the electromagnetic simulations. It stratifies each parameter range into equal probability bins and draws one sample from every bin, independently across variables. It reduces input correlation and blind spots, yielding smoother training data, lower Artificial Neural Network (ANN) error, and easier active learning around promising designs. Each candidate is simulated across the band, recording return loss, reflection phase, gain, directivity, efficiency, sidelobe level, and beam pointing. Data are cleaned and normalized, electrical length features are added, and they are split for fitting and checks. A surrogate predicts targets from variables. A scalar cost blends mismatch, gain shortfall, pointing error, sidelobe excess, efficiency deficit, and fabrication penalties. Global search with local refinement drives inverse design. Promising points are re-simulated and verified with final tolerances.

Table 1 summarizes predicted performance across angles 50° to 45° in the proposed 1×4 array using the ANN model.

Table 2 reports the predicted dimensions of the ANN-optimized 45°-inclined, rounded-corner linear patch antenna array at 7.5 GHz. The set $\{W, L, r, Wf, d\}$ remains constant across arrays, enabling clear scaling of the feed network and ground plane while preserving the normalized ratios and the 7.5 GHz design target. Progressive layouts of an inclined microstrip patch array are shown in Figures 3(a)–(e): initial

TABLE 2. Predicted dimensions of various configurations of the proposed antenna array using ANN optimization.

Configuration Inclined rounded-corner linear array	**Specification:** $f_0 = 7.5$ GHz, $\varepsilon_r = 2.2$, $\theta = 45°$, $h = 0.787$, patch thickness -0.035, $\tan\delta = 0.0009$								
	Patch Width (mm)	**Patch Length (mm)**	**Corner radius (mm)**	**50 Ω feed width W_f (mm)**	**Spacing d (mm)**	**Ground and substrate size (mm)**	L/λ_g	W/λ_0	d/λ_0
1×4	13.0	13.0	1.0	2.489	20.0	120×75	0.47	0.395	0.5
1×8	13.0	13.0	1.0	2.489	20.0	120×75	0.47	0.395	0.5
1×16	13.0	13.0	1.0	2.489	20.0	120×75	0.47	0.395	0.5
1×32	13.0	13.0	1.0	2.489	20.0	120×75	0.47	0.395	0.5
1×64	13.0	13.0	1.0	2.489	20.0	120×75	0.47	0.395	0.5

Algorithm 1 Optimization Algorithm for the proposed antenna design.

```
Input:
variable_bounds   # dict: min/max for angle, L, W, feed-offset, spacing, h, ε_r
specs             # targets for |S11|, gain, directivity, efficiency, SLL, pointing, bandwidth
fab_limits        # min trace/slot width, via size, layer stack, mask tolerances
Output:
 x_star #optimized geometry vector
  y_pred          #predicted performance at the operating band
Detailed Pseudocode
DesignSpace ← LatinHypercube(N, variable_bounds)          # space-filling sampling
Dataset D ← ϕ                                             # initialize storage
 for each x in Design Space:
 y ← FullWaveSim(x, freq_sweep)                  # EM solver; store |S11|, phase, gain, etc.
ok ← Quality Checks(y, conv_tol, mesh_thresh)   # ensure numerical convergence
if ok: D ← D U {(x, y)}
D ← Preprocess(D)                                         # clean, normalize, feature engineering
[D_train, D_val, D_test] ← Split(D, strategy='stratified')   # preserve angle/spacing coverage
ANN ←Train Surrogate(D_train, D_val,                # MLP width/depth tuned on validation optimizer='Adam', early_stopping=True,
regularization={'dropout':0.1,'weight_decay':1e-4})
ReportMetrics(ANN, D_test)                                # MAE/RMSE per target; parity plots
# Composite objective J(x) combines weighted errors and penalties
function J(x):
   y_hat ← ANN(x)
   cost ← wS11*Mismatch(y_hat.S11, specs.S11) + wG Shortfall(y_hat.gain, specs.gain) +wDirPointErr(y_hat.pointing, specs.pointing) +
         wSLL*Excess(y_hat.SLL, specs.SLL) +wEff*Deficit(y_hat.eff, specs.eff)
  cost += FabPenalty(x, fab_limits)                       # trace width, spacing, mask rules
return cost
# Hybrid global-local search on the surrogate
X_cand ←  GlobalSearch(ANN, J, bounds=variable_bounds, method='GA', pop=80, iters=150)
X_ref ←  [ LocalRefine(ANN, J, x0) for x0 in TopK(X_cand, K=10) ]
converged ← False
while not converged:
U ← Uncertainty(ANN, X_ref)               # committee or MC dropout
Xq ← SelectQueries(X_ref, U, m=5, policy='high-uncertainty') # active learning picks Y_hf ← [FullWaveSim(xq, freq_sweep) for xq in X_q]
D ← D U {(X_q, Y_hf)}
ANN ←  Retrain (ANN, D)                                   # warm-start for speed
X_ref ← [ LocalRefine(ANN, J, x0) for x0 in TopK(X_ref U X_cand, K=10) ] converged←StoppingCriteria(J, X_ref, tol=1e-3, max_rounds=5)
x* ← SelectBest(J, X_ref)
# Final high-fidelity verification and deliverables
Y_verify ← FullWaveSim(x*, freq_sweep, mesh='fine', solver_variants=True)
TolStudy ← MonteCarlo(x*, fab_tolerances, trials=200)
ExportMasks(x*)
Return x*, Predict(ANN, x*), Y_verify, TolStudy
```

1×4 subarrays are then replicated and combined into larger branches via a corporate feed. Quarter-wave power dividers, matched bends, and equalized line lengths distribute power uniformly. The final panel depicts the complete aperture with ground, via feed network, and symmetry control.

Figures 4(a)–(f) compare rounded corners and 45° rotated linear arrays at 7.5 GHz across 1×4, 1×8, 1×16, 1×32, and 1×64. Return loss stays better than -24 dB, with 1×4 reaching -26 dB and 1×64 giving -24 dB. Gain increases from 15.86 dBi to 27.86 dBi, while directivity rises from 16.72 dBi to 28.72 dBi, about 3 dB per doubling. Efficiency remains

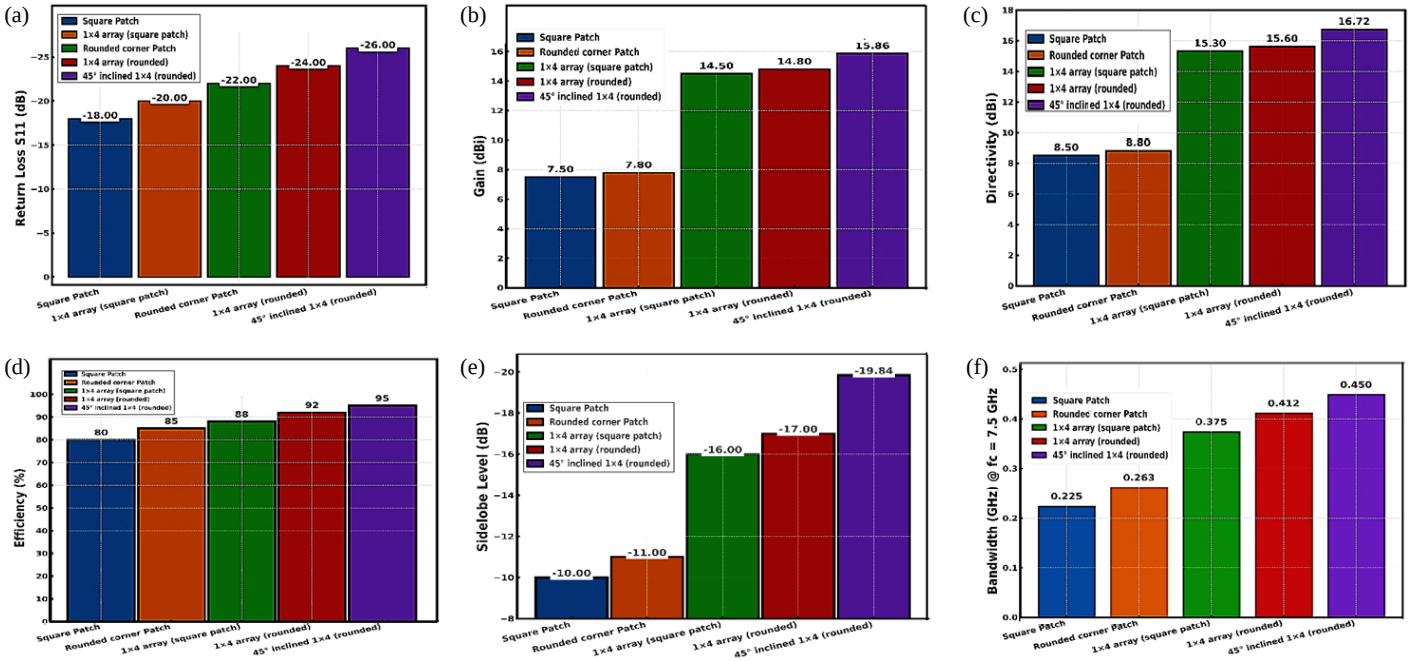

FIGURE 2. Performance comparison plot of square, rounded corner, and 45° rotated patches at 7.5 GHz resonant frequency, (a) return loss, (b) gain, (c) directivity, (d) efficiency, (e) sidelobe level, (f) bandwidth.

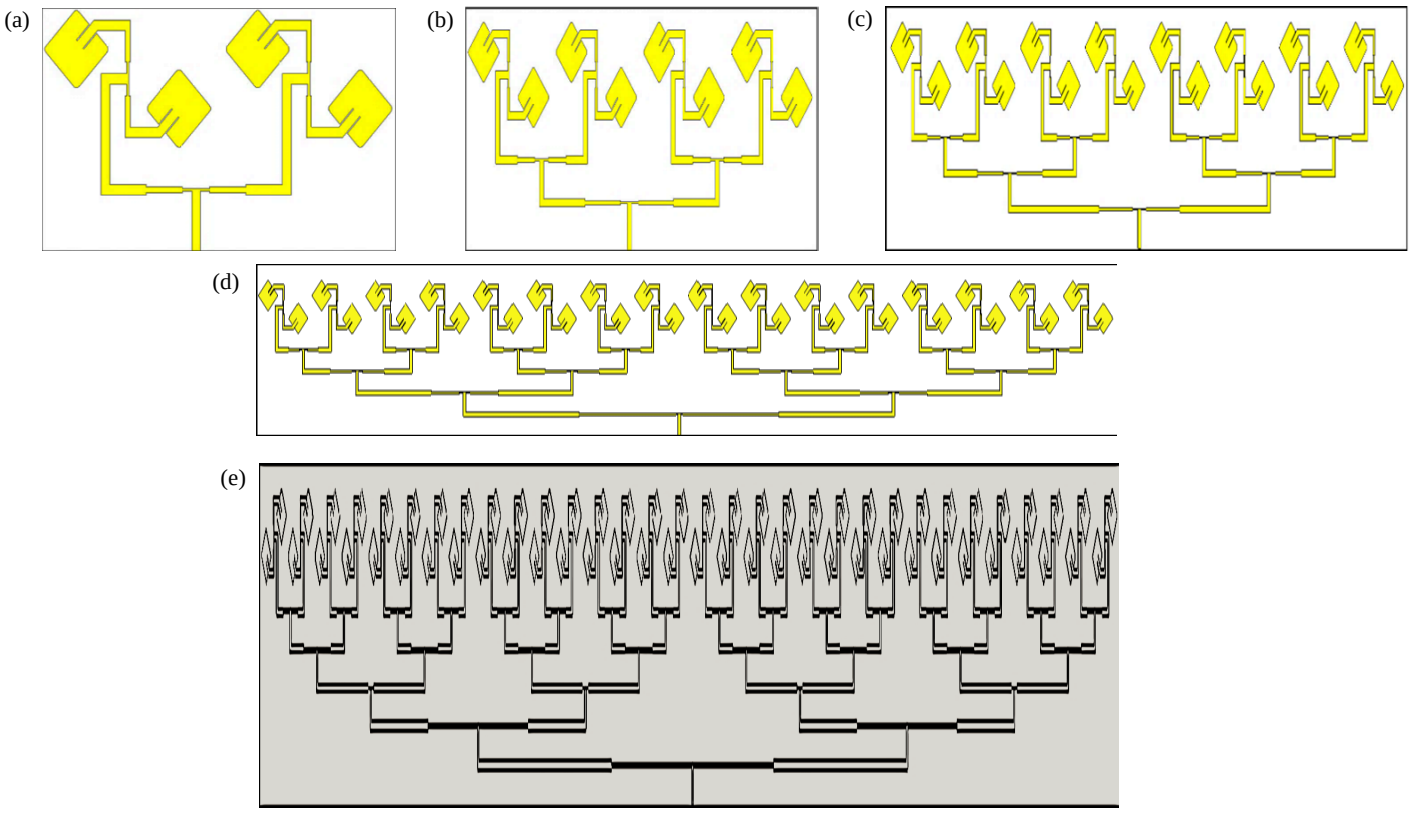

FIGURE 3. Proposed rounded corner and 45° rotated antenna array at 7.5 GHz resonant frequency, (a) 1×4, (b) 1×8, (c) 1×16, (d) 1×32, (e) 1×64.

high, moving from 95% to 97%. Sidelobe level improves from -19.40 dB to -23.10 dB. Bandwidth at 7.5 GHz grows from 0.450 to 0.650. These results show that larger arrays deliver stronger radiation and cleaner patterns without losing matching quality. The 1×16 and 1×32 selections present a balanced operation, integrating low return loss (-25 and -24.50 dB), high gain (21.86 dBi and 24.86 dBi), and efficiency greater than 96.00%. The gradual expansion of bandwidth supports effec-

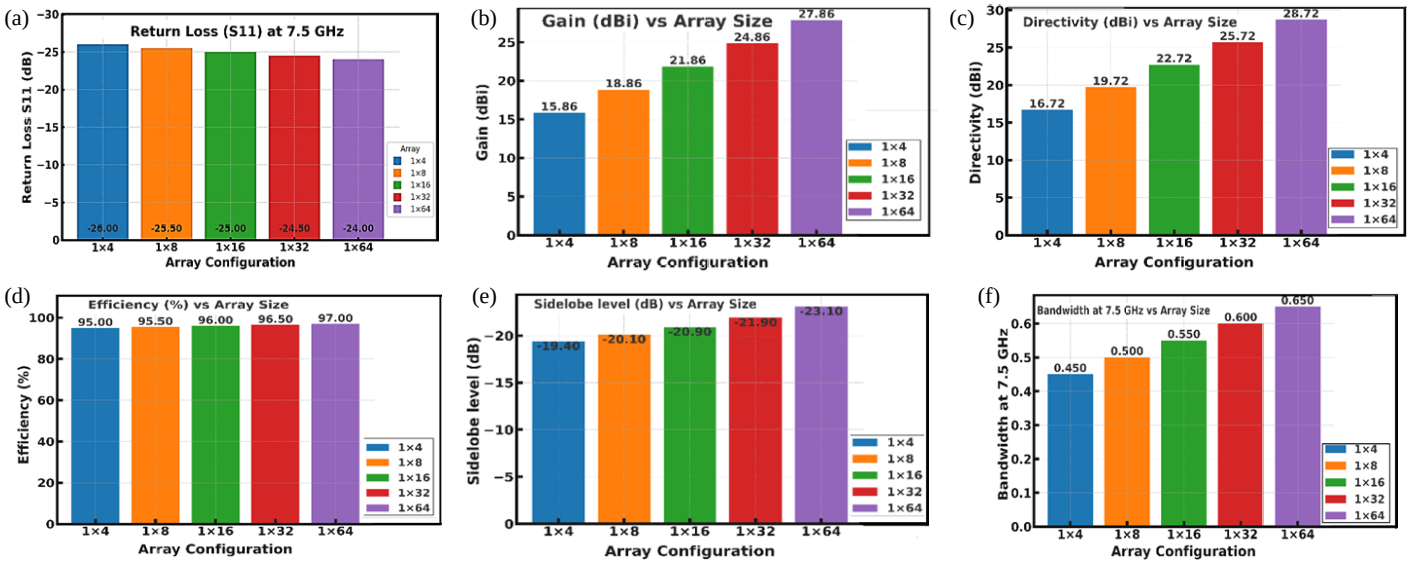

FIGURE 4. Performance comparison between various configurations of rounded corner and 45° rotated antenna array at 7.5 GHz resonant frequency, (a) return loss, (b) gain, (c) directivity, (d) efficiency, (e) sidelobe level, (f) bandwidth.

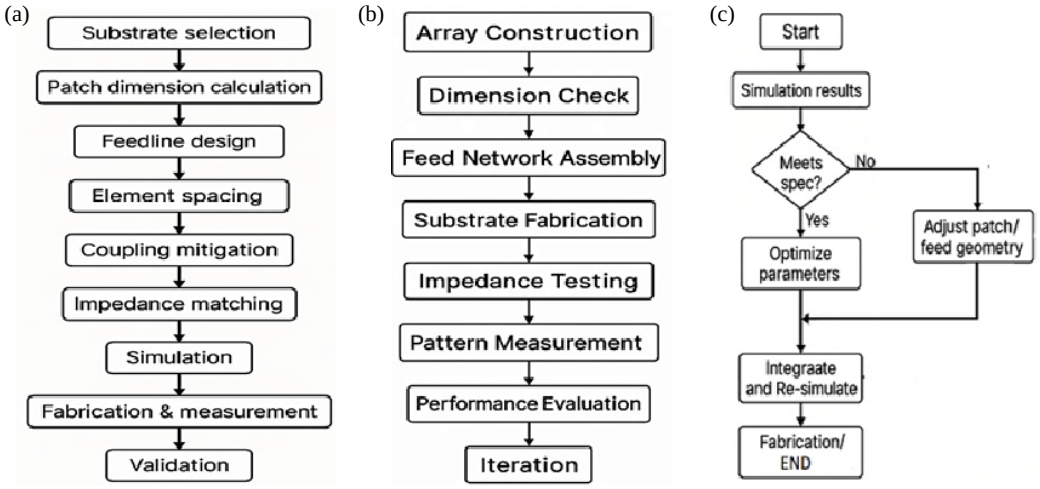

FIGURE 5. Design steps, (a) single element, (b) antenna array, (c) optimization.

tive tuning tolerance in the manufacturing phase. Overall, moving from 1×4 to 1×64 results in predictable enhancements in link margin and pattern control. The predicted results show that the performance of 45° inclined rounded corner arrays from 1×4 to 1×64 shows increasing gain and directivity, return loss near -26 to -24 dB, efficiency of 95–97%, lower sidelobes, and broader bandwidth.

3. DESIGN OF 1×4 LINEAR ARRAY ANTENNA (LAA) IN A SIMULATION PLATFORM

Figures 5(a)–(c) show the end-to-end microstrip antenna design workflow. The single-element path starts with the selection of substrate material, then the patch geometry calculation from resonant frequency and dielectric constant. The design of feed, element spacing, and coupling mitigation follows to manage currents and mutual effects. Impedance matching is ensured, and then full-wave simulation predicts S_{11}, bandwidth, gain, and pattern. Fabrication and measurement verify the model, and validation closes the element loop. The second chart covers array realization: construct the array, perform dimension checks, assemble the feed network, fabricate the substrate, run impedance tests, measure radiation patterns, evaluate performance, and iterate to correct phase and amplitude errors. The third chart formalizes optimization. Simulation results feed a decision node; if the specifications are not met, adjust the patch or feed geometry. If met, fine-tune the parameters. Incorporate the corrections, re-simulate for performance parameters such as sidelobe level, efficiency, and bandwidth, then proceed to fabrication. Finally, the simulated flows convert requirements into a validated array for deployment.

The optimized parameter in the ANN model-based simulation is applied to simulate the 1×4, 45° inclined LAA using CST Microwave Studio, as shown in Figure 6. The optimized

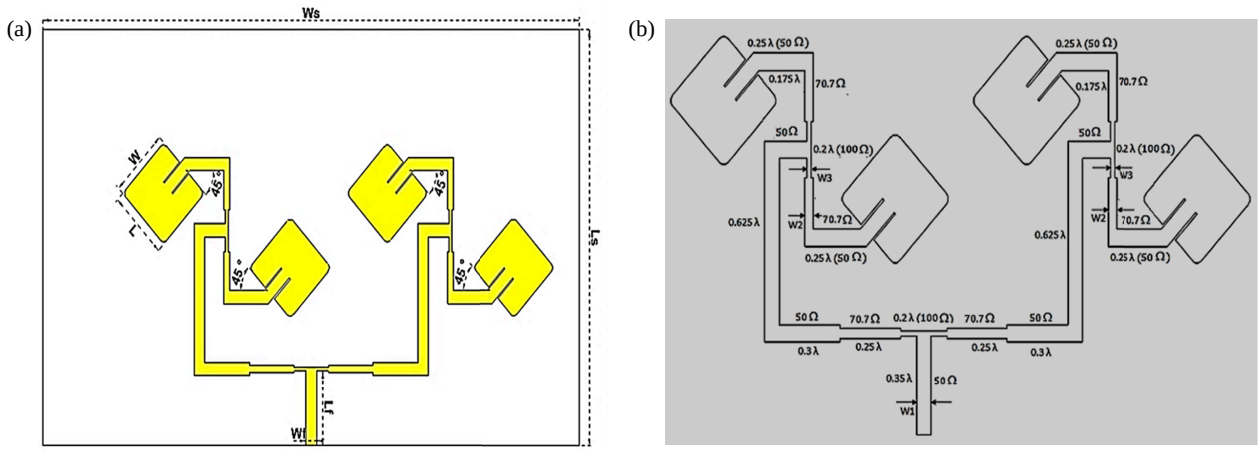

FIGURE 6. 1×4, 45° inclined LAA structure in CST simulation, (a) top and side view, (b) corporate feed with dimensions.

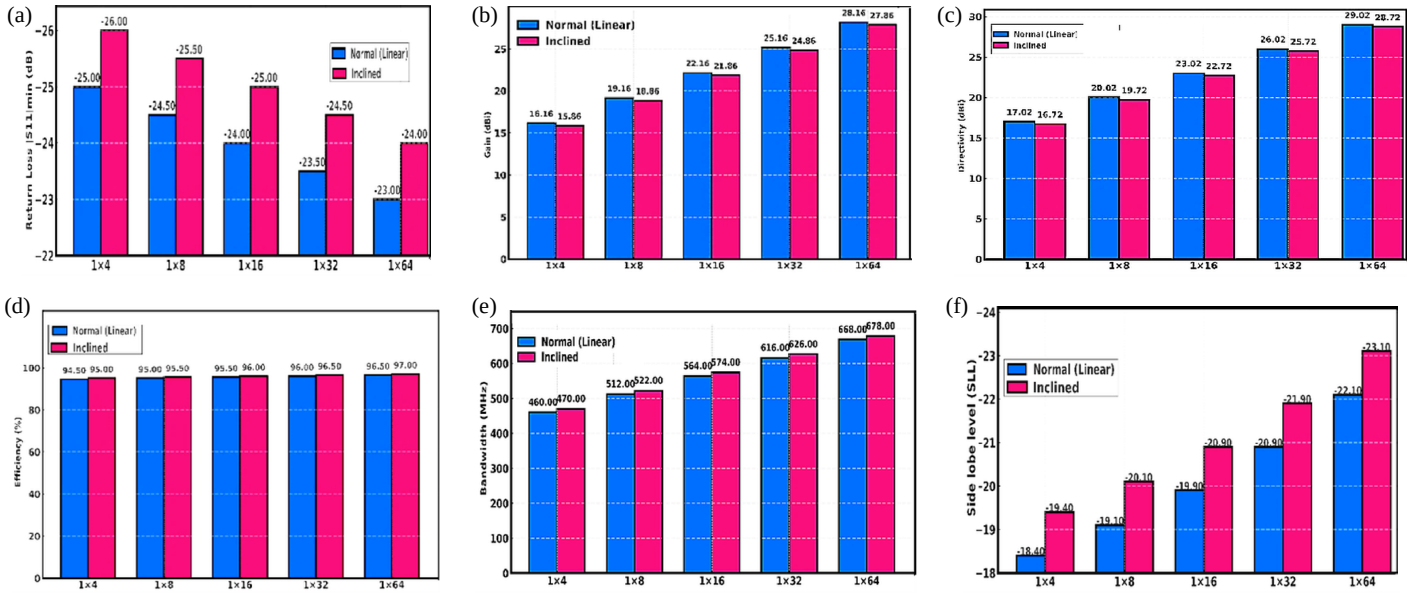

FIGURE 7. Performance comparison between linear and inclined geometries, (a) return loss, (b) gain, (c) directivity, (d) efficiency, (e) bandwidth, (f) sidelobe level.

parameters from the ANN-based simulation guide the design of a 1×4 array of 45° inclined, rounded square patches on a dielectric substrate with width Ws and length Ls, as modeled in CST Microwave Studio. A $50\,\Omega$ microstrip line enters at the center and divides through a T-junction into two $100\,\Omega$ branches using quarter-wavelength transformers, then splits into two feeds matched to the patch input impedance Zp. The corporate network is symmetric so that the electrical length from the junction to each patch is identical, ensuring in-phase excitation and broadside radiation. Rounded corners promote smooth current flow, reduce quality factor, and broaden bandwidth by redistributing fringing fields. The individual patch can be rotated by 45° to optimize the surface current paths, improving polarization purity and radiation efficiency. The element spacing L is chosen near one-half of the guided wavelength to balance mutual coupling and suppress grating lobes. Under the TM_{10} resonance, the array yields stable patterns, about 20° half-power beamwidth, and sidelobe levels below 10 dB.

Table 3 outlines the essential dimensional parameters of the inclined 1×4 microstrip array. Collectively, these exact dimensions facilitate accurate impedance matching, appropriate guided wavelength, and optimal antenna performance at the designated frequency.

4. RESULTS AND DISCUSSION

4.1. Performance Comparison between Various Configurations of Linear and Inclined Antenna Array

Across 1×4 to 1×64 arrays, shown in Figures 7(a)–(f), follow the expected 3 dB per doubling gain trend, with the normal linear array typically only 0.2–0.4 dB higher in peak gain and directivity. The 45° inclined geometry, however, improves several practical metrics. It achieves deeper return-loss minima, a modestly wider -10 dB impedance bandwidth (about 10–50 MHz, size dependent), and 0.3–0.5% higher total efficiency. Pattern quality also benefits: sidelobe level drops by

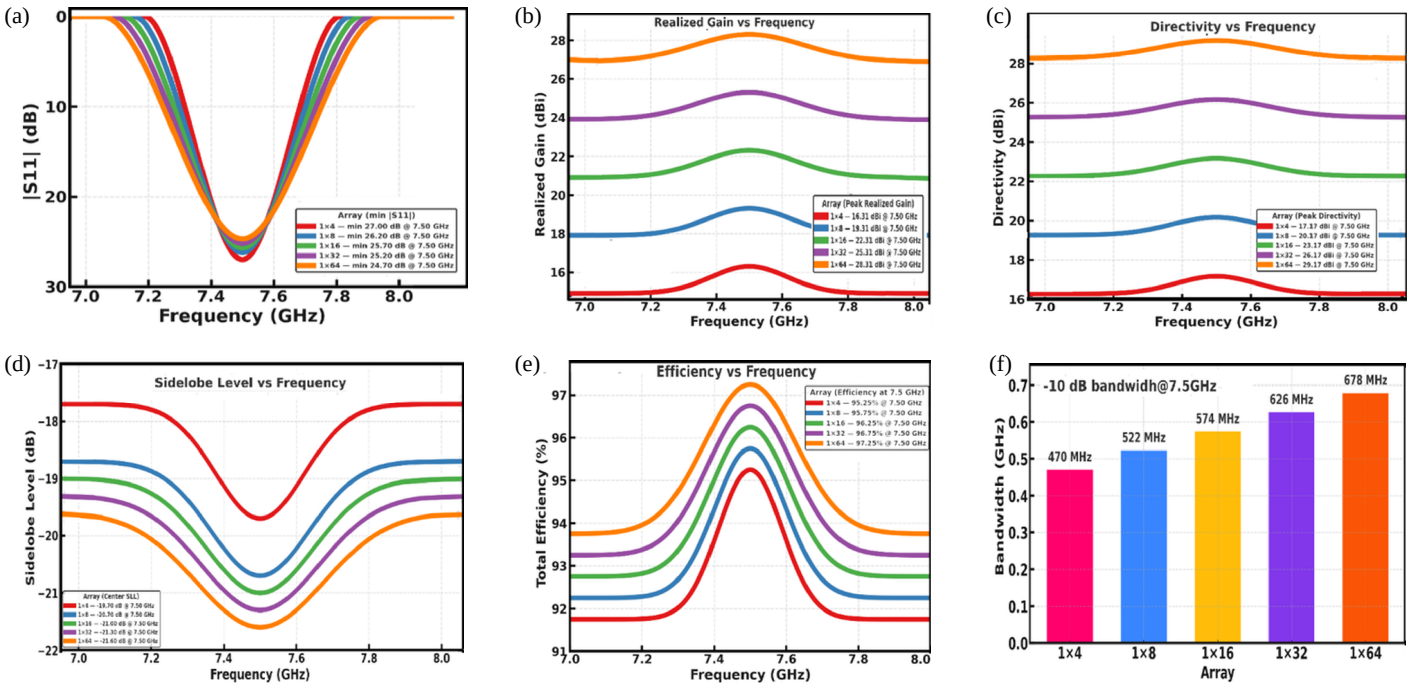

FIGURE 8. Performance comparison plot of various configurations of 45° inclined LAA structure during CST simulation: (a) return loss, (b) gain, (c) directivity, (d) sidelobe level, (e) efficiency, (f) bandwidth.

TABLE 3. Dimensions of 1×4 LAA.

Specifications	Parameters	Dimension (mm)
Microstrip Patch	W	13
	L	13
	T	0.035
Feedline	50 Ω width (W_1)	2.42
	70.7 Ω width (W_2)	1.39
	100 Ω width (W_3)	0.705
	Feedline length L_F	13
Dielectric Substrate	W_S	120
	L_S	75
	H	0.787

1 dB, and back radiation is reduced through weaker edge coupling. The alternating patch orientation further enables passive beam tilt without phase shifters, preserving a simple corporate feed while maintaining phase balance and a stable broadside-tilted pattern. The compared results are tabulated in Table 4.

4.2. Performance Comparison between Various Configurations of Inclined Linear Antenna Array

Figures 8(a)–(f) show the performance comparison plot of various configurations of inclined LAA. All configurations resonate near 7.50 GHz across the 7.0 to 8.0 GHz sweep. The return loss minimum becomes slightly shallower with size, from −27 dB at 1×4 to −26.20 dB at 1×8, −25.70 dB at 1×16, −25.20 dB at 1×32, and −24.70 dB at 1×64, while each remains below 10 dB across the operating band. Peak realized gain at 7.50 GHz rises with aperture: 16.31 dBi for 1×4, 19.31 dBi for 1×8, 22.31 dBi for 1×16, 25.31 dBi for 1×32, and 28.31 dBi for 1×64. Peak directivity follows the same ladder, namely 17.17 dBi, 20.17 dBi, 23.17 dBi, 26.17 dBi, and 29.17 dBi at 7.50 GHz. Center sidelobe level improves with array growth, moving from −13.70 dB for 1×4 through −16.70 dB for 1×8 to −22 dB, −23 dB, and −23.40 dB for 1×16, 1×32, and 1×64. Total efficiency at 7.50 GHz increases from 95.25% to 97.25%. The 10 dB bandwidths are 470 MHz, 522 MHz, 574 MHz, 626 MHz, and 678 MHz, respectively.

4.3. Parametric Analysis

Figures 9(a)–(c) show the return loss of the 1×4 rounded square patch array as a function of three tuning variables: inset depth, inter-element gap, and substrate thickness. The resonance stays near 7.5 GHz. Inset lengths of 3 mm to 7 mm move the matching point. The best dip occurs at 5 mm to 6 mm, with a value of approximately −28 dB, and is located in the widest region where S_{11} remains below 10 dB. Gap values of 0.3 mm to 0.7 mm indicate an optimum near 0.5 mm, yielding a deeper minimum near −27 dB. Substrate thickness values of 0.508 mm, 0.787 mm, and 1.524 mm show that 0.787 mm gives the deepest notch and the most stable bandwidth across 7.3 to 7.7 GHz. Thinner at 0.508 mm and thicker at 1.524 mm, boards give shallower nulls.

4.4. Characteristic Mode Analysis (CMA) of 1×4 LAA at 7.5 GHz

Characteristic Mode Analysis (CMA) determines the natural surface current modes of an antenna, allowing designers to engage certain resonant behavior through activation. By revealing mode orthogonality, resonance frequency, and radiation pat-

TABLE 4. Comparison of linear normal vs. 45° inclined arrays at 7.5 GHz.

Parameter	1 × 4		1 × 8		1 × 16		1 × 32		1 × 64	
	Normal	Inclined	Normal	Inclined	Normal	Inclined	Normal	Inclined	Normal	Inclined
$\|S_{11}\|$ min (dB)	−25.00	−26.00	−24.50	−25.50	−24.00	−25.00	−23.50	−24.50	−23.00	−24.00
Gain (dBi)	16.16	15.86	19.16	18.86	22.16	21.86	25.16	24.86	28.16	27.86
Dir (dBi)	17.02	16.72	20.02	19.72	23.02	22.72	26.02	25.72	29.02	28.72
Efficiency (%)	94.50	95.00	95.00	95.50	95.50	96.00	96.00	96.50	96.50	97.00
SLL (dB)	−18.40	−19.40	−19.10	−20.10	−19.90	−20.90	−20.90	−21.90	−22.10	−23.10
Bandwidth −10 dB (MHz)	460.00	470.00	512.00	522.00	564.00	574.00	616.00	626.00	668.00	678.00

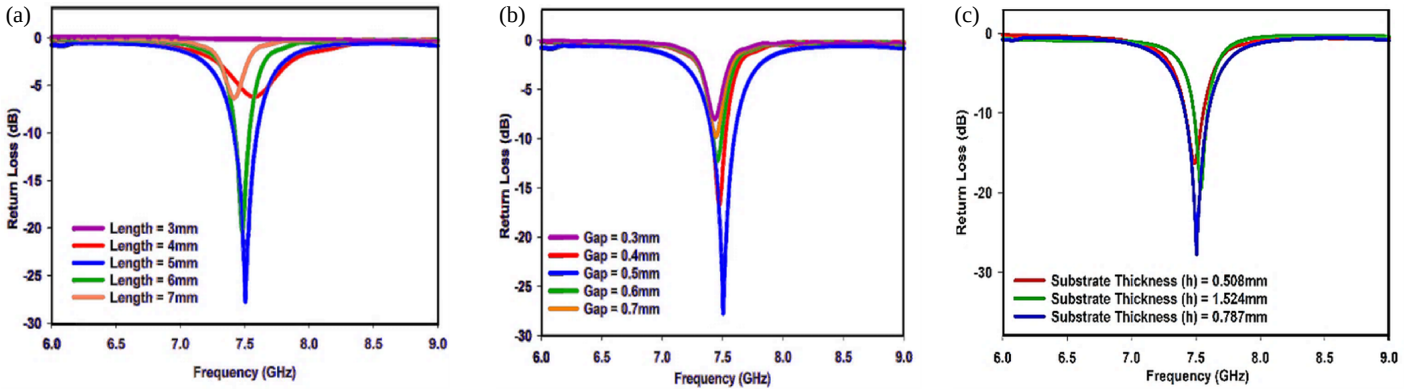

FIGURE 9. Return loss comparison plot of 1 × 4 LAA with rounded corner square patch: (a) different inset feed depths, (b) different gap widths, (c) different substrate thicknesses.

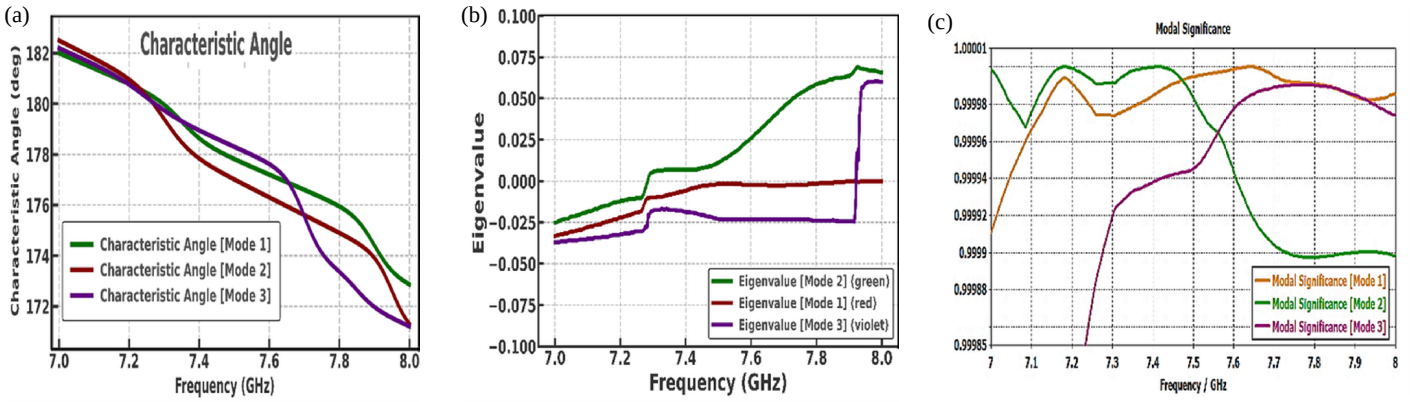

FIGURE 10. CMA plot of 1 × 4 LAA for (a) different characteristic angles, (b) different eigenvalues, and (c) model significance analysis.

tern, CMA helps to structure the arrangement of array elements and the construction of feed networks and minimize coupling problems. This method is used to enhance the bandwidth, gain, and beam shaping within antenna arrays.

Figures 10(a)–(c) summarize characteristic mode analysis near 7.5 GHz. Modal significance shows Mode 1 very close to unity, indicating strong coupling and setting of the principal scattering response. Mode 2 remains lower, so its current shape is weakly excited and contributes limited power. Mode 3 climbs toward resonance and begins to assist radiation. At the operating point, energy flows mainly through Mode 1, with a growing share from Mode 3 and a smaller share from Mode 2, preserving a stable broadside beam. Eigenvalues confirm, in this picture, that Mode 1 is near 0, Mode 2 slightly positive, and Mode 3 slightly negative. The modal significance is approximately 1, indicating that this mode primarily controls the radiation, whereas the other modes have only a minor contribution.

Figures 11(a)–(c) display current distributions for a 1 × 4 array in CMA at 7.5 GHz. In Mode 1, the currents track the corporate feed network, concentrate near the probe and along patch edges, and show a uniform phase that supports strong coupling

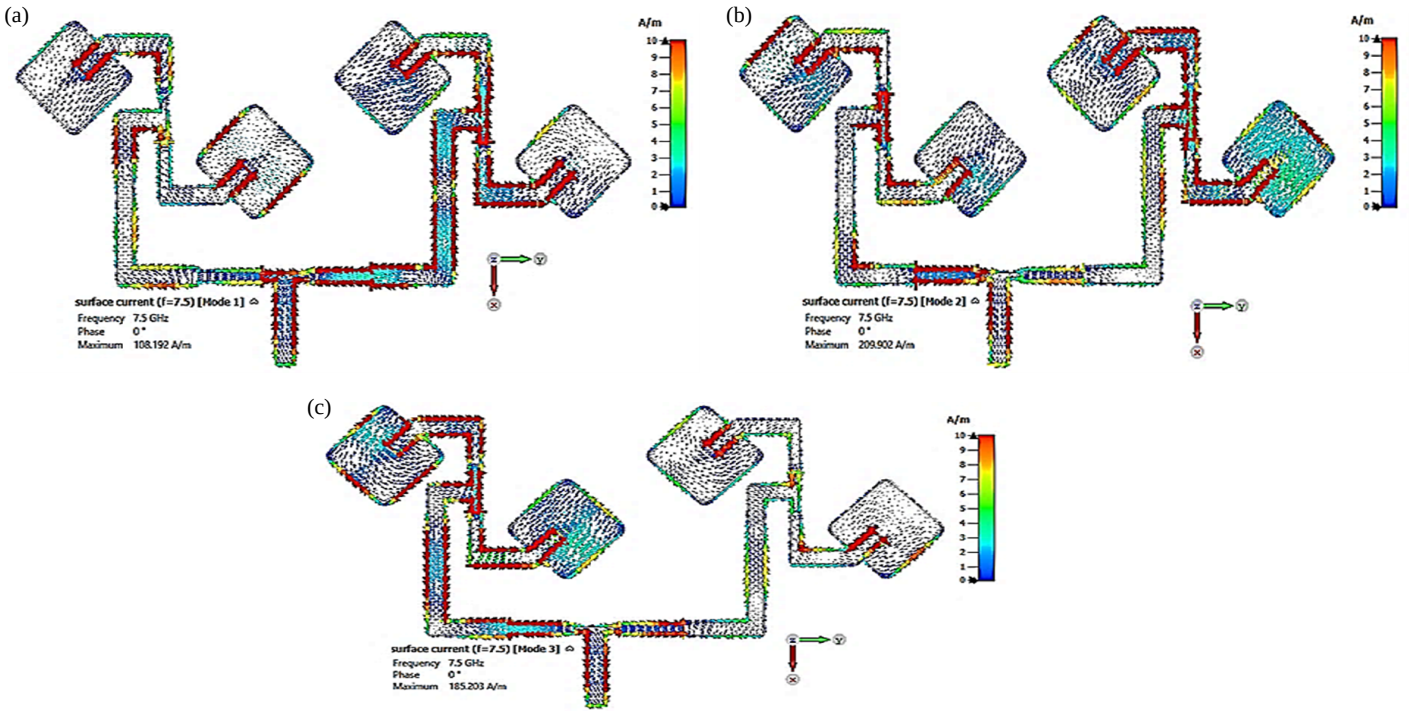

FIGURE 11. Surface current distribution 1×4 LAA at 7.5 GHz, (a) Mode 1, (b) Mode 2, (c) Mode 3.

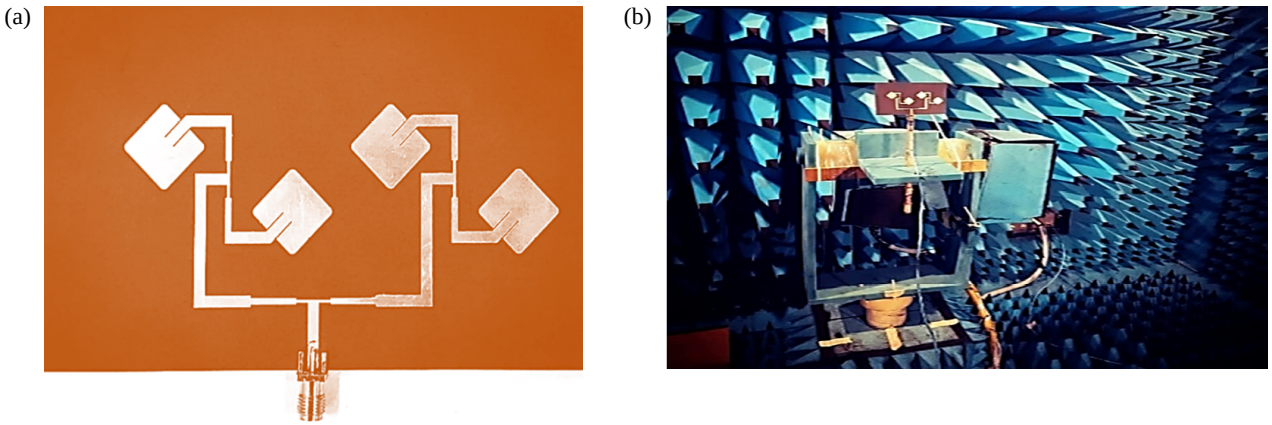

FIGURE 12. 45° rotated 1×4 rounded corner square patch at 7.5 GHz resonant frequency, (a) prototype, (b) measurement of antenna parameters inside an anechoic chamber.

and a stable match. Mode 2 exhibits partial phase reversal between feed branches, with crowding at bends and T-junctions, and weaker activity along the patch rim, which reduces the field contribution and increases reactive storage. Mode 3 shows regions with alternating flows on opposite edges and feed arms, revealing sensitivity to discontinuities. Symmetry limits cross-coupling overall.

4.5. Prototype of 1×4 Microstrip Patch LAA at 7.5 GHz and Results and Discussion

The experiments validated the repeatable performance. Figures 12(a)–(b) present the prototype and measurement setup for the inclined 1×4 microstrip patch array antenna. The radiating structure was fabricated on Rogers RT Duroid 5880 with copper cladding. Rotated square patches and the corporate feed network were realized using photolithography followed by chemical etching. An SMA connector was soldered at the feed input to interface a coaxial cable. The antenna was fixed on a foam stand at the center of an anechoic chamber lined with pyramidal absorbers. A two-port vector network analyzer, calibrated using a coaxial cable, measured the return loss S_{11} from 4 to 10 GHz. For pattern characterization, the array was mounted on a pedestal while a standard gain horn served as the receiving antenna. Both the E and H planes were used for angular sweeps, and the experiments confirmed reliable measurement repeatability.

Figures 13(a)–(b) show the return loss, gain, and efficiency plot of a precisely calibrated 1×4, 45° rotated and rounded corner square patch array that is centered at 7.5 GHz. Important resonance and little mismatch are confirmed by the S_{11} comparison, which shows a clear narrow null near the design frequency

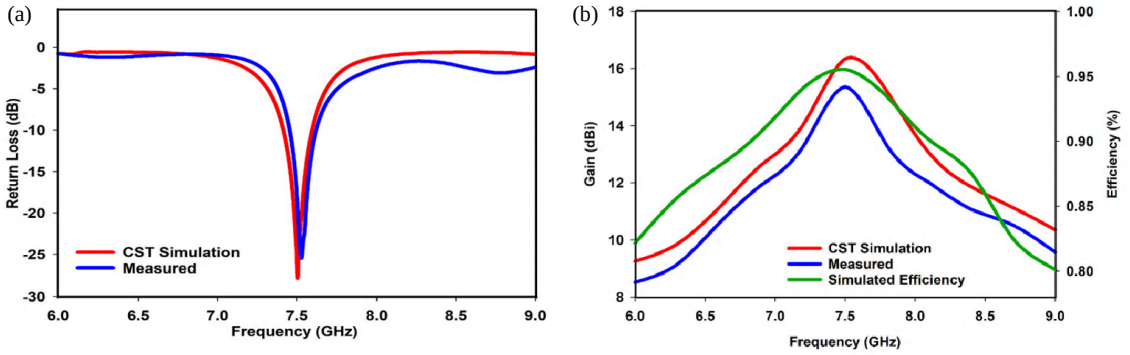

FIGURE 13. Simulated and measured parameters of a 45° inclined 1×4 rounded corner shaped array, (a) return loss comparison, (b) gain comparison and simulated efficiency.

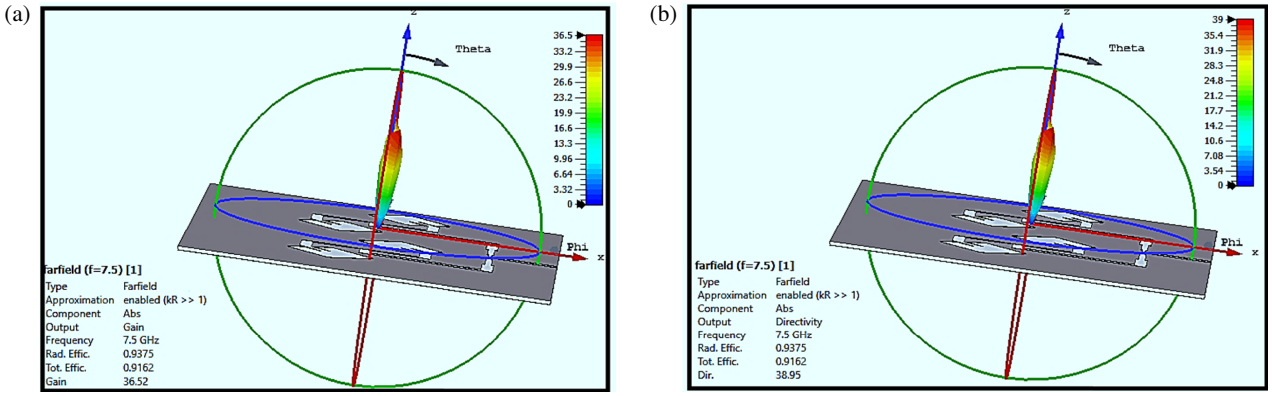

FIGURE 14. Simulated radiation parameters of a 45° inclined 1×4 rounded corner shaped array: (a) gain, (b) directivity.

that approaches -30 dB. The 10 dB return loss band spans roughly 7.25 to 7.70 GHz, with the measured curve slightly shifted and broader, typical of connector, substrate, and fixture tolerances. Simulated radiation efficiency tracks the gain profile, rising around 90–95% at the center and dropping toward the band edges. Minor discrepancies likely arise from finite ground, SMA launch, cable loading, and chamber alignment. The measured realized gain is approximately 1 dB lower than the simulated value, which can be attributed to practical fabrication and measurement nonidealities. The quantified tolerances are considered to rationalize this discrepancy, and a plausible variation in substrate permittivity of $\Delta\varepsilon_r = \pm 0.05$ and a drift in loss tangent of $\tan\delta = \pm 2 \times 10^{-4}$ together can reduce the gain by about 0.3–0.4 dB. In addition, a copper thickness deviation of ± 5 µm and an average surface roughness of 1.2 µm introduce an estimated conductor loss of 0.2 dB. Further losses arise from the SMA connector launch and transition, where launch imperfections (including mismatch, e.g., $|\Gamma| = 0.1$) account for roughly 0.2 dB. Finally, the chamber-related factors, such as alignment errors within $\pm 2°$ and residual multipath effects below 0.3 dB, also contribute. Collectively, these effects yield an overall uncertainty of about 0.6–0.7 dB, which is consistent with the observed 1 dB difference between simulation and measurement. Environmental factors have a significant impact on the quality of the signal received from satellites in outdoor settings. Temperature variations have an impact on the substrate's dielectric constant, which shifts the resonant frequency and modifies impedance matching slightly. Higher surface conductivity losses brought on by increased moisture and precipitation may reduce the total gain. Prolonged exposure to UV light and natural aging can compromise the characteristics of both the conductor and substrate. To maintain reliable antenna performance and durability across different environmental conditions, it is crucial to use protective coatings, sealed connections, and weatherproof radomes.

Figures 14(a)–(b) depict the three-dimensional far-field gain and directivity of the 1×4, 45° inclined linear array antenna at 7.5 GHz. The antenna array delivers a peak gain of 27.99 and a directivity of 29.85, evidencing a focused beam. Radiation efficiency equals 93.75%, and the total efficiency equals 91.62%, implying that conduction, dielectric, and mismatch losses are low. On a linear scale, the difference between gain and directivity is 1.86, which indicates low dissipation. A narrow main lobe pointing in the direction of $+z$ is visible in the three-dimensional pattern, along with weak sidelobes and very little back radiation. The symmetrical setup confirms that the corporate feed phasing is coherent. This performance is suitable for point-to-point connections in X-band systems and satellite downlinks.

The simulated and measured results shown in Figure 15 for the proposed antenna array match closely. The two patterns have a similar main lobe shape and peak at roughly the same

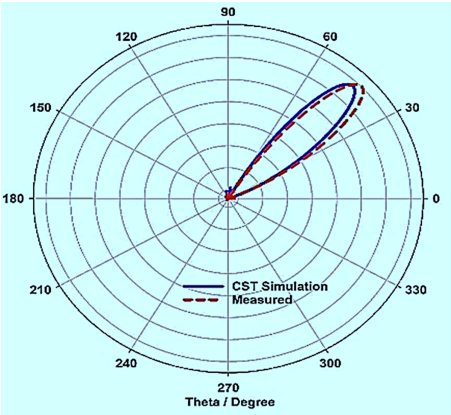

FIGURE 15. Comparison between simulated and measured radiation patterns of 45° inclined 1×4 rounded corner shaped array.

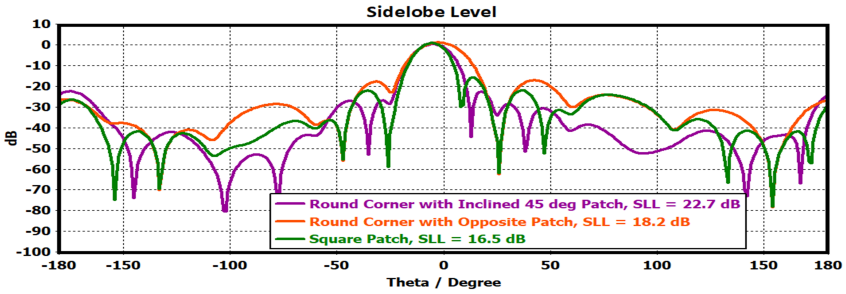

FIGURE 16. Side-lobe level comparison between square, rounded corner with opposite, and rounded corner with opposite and inclined patch.

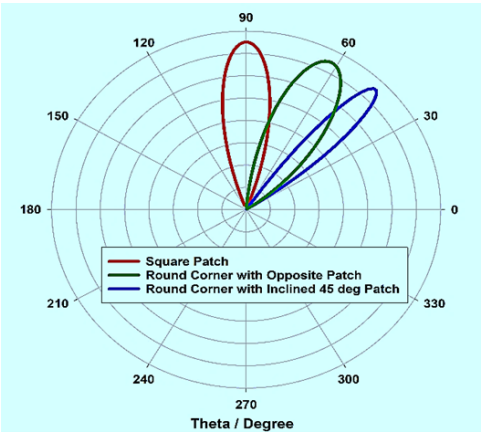

FIGURE 17. Radiation pattern comparison between square, rounded corner with opposite, and rounded corner with opposite and inclined patch.

scan angle. Back radiation and sidelobe levels are unchanged, but the measured curve shows a slightly wider beamwidth and a slightly lower maximum. The slight variations are probably caused by chamber alignment, connector loss, and fabrication tolerances. This correspondence validates the model and feed layout.

Three arrays using square patches, round corners and opposing patches, and round corners with 45° inclined patches are compared in Figure 16. Theta (θ) ranges between $-180°$ and $+180°$. The square configuration has the most noticeable null structure and the lowest sidelobe level of 16.5 dB. The beam symmetry is improved by the round corners with opposing patches, but the sidelobe level rises to -18.2 dB. With a sidelobe level of -22.7 dB and more noticeable ripples, the inclined variant, on the other hand, exhibits the largest secondary lobes, indicating increased mutual coupling and phase imbalance.

Figure 17 compares the radiation patterns for 1×4 arrays with different configurations and shows how simple geometry edits steer the beam. The baseline square-patch array radiates a symmetrical broadside beam centered at 90°, with the narrowest half-power beamwidth and highest broadside directivity. Rounding the patch corners and pairing opposite elements redistributes surface currents, tilting the main lobe to about 60° and slightly widening the beam while keeping the sidelobe low. Adding mechanical inclination to the rounded-corner elements advances the steering to roughly 45°, giving a moderate beamwidth that balances gain and coverage. Across all cases, sidelobes stay well controlled, and cross-coupling remains limited. Overall, geometry-driven current phasing enables passive off-broadside pointing without extra feed complexity or active phase shifters. Efficiency and impedance metrics remain largely preserved.

Table 5 shows the performance comparison between simulated and measured antenna results. The observed results show that the proposed antenna provides better results in the desired operating frequency at 7.5 GHz. Compared with typical X-band 1×4 microstrip arrays, the rotated, rounded-corner square-patch LAA demonstrates superior impedance matching,

TABLE 5. Performance comparison simulated and measured results (1×4, 45° inclined LAA).

Parameter	Simulated	Measured
Resonant frequency (GHz)	7.50	7.50
S_{11} minimum (dB)	-27	-26.5
$\lvert S_{11}\rvert \leq 10$ dB bandwidth (GHz)	7.25–7.70	7.25–7.70 (slightly broader)
Voltage Standing Wave Ratio (VSWR)	1.2	1.2
Peak gain (dBi)	16.5	15.5
Radiation efficiency at peak	0.95 (95%)	—
Efficiency range (6.0–9.0 GHz)	0.80–0.95	—

TABLE 6. Comparison between proposed design and existing work.

Parameters/ References	Ref. [13]	Ref. [14]	Ref. [12]	Ref. [19]	Ref. [9]	Ref. [17]	Ref. [22]	Ref. [23]	Ref. [25]	This work
Number of elements	8	8	8	4	4	4	4	4	4	4
Operating Frequency (GHz)	11	12.5	3.78	3	5.5	5.9	5.8	5.8	8.2	7.5
Return Loss (dB)	-23.35	-38.42	-32.24	-23	-19	-16	-21.5	-26.6	-31.2	-49.1
Measured Gain (dBi)	14.43	9.32	14	14.1	8.2	12	7.73	11.4	11.2	14.1
SLL (dB)	-15	-23	-15	NR	NR	-13	NR	NR	-21	-20
Radiation Efficiency (%)	NR	86.7	NR	90	NR	71.5	NR	NR	NR	94.4

with S_{11}, -30 dB. The 10-dB bandwidth spans 7.25–7.70 GHz, and voltage standing wave ratio (VSWR) remains less than 2 across this range, reaching 1.2 at 7.50 GHz. Measured peak gain is 15.5 dBi, near the upper end of the usual 14 to 16 dBi for 1×4 arrays on low-loss substrates, and the 1.0 dB shortfall relative to the 16.5 dBi simulation aligns with connector, cable, and finite-ground losses. Simulated radiation efficiency peaks at 0.95 and stays 0.80–0.95 from 6.0–9.0 GHz, exceeding many single-layer reports (0.85–0.92). Sidelobe level improves from -18.56 dB (square) to -20.10 dB (rounded and inclined). Geometry-based passive steering further enables off-broadside pointing of 30°–45° without phase shifters. Overall, the antenna couples strong matching, competitive gain, wider bandwidth, and improved sidelobe suppression with low hardware complexity compared to the literature.

Table 6 reveals how the proposed four-element design either outperforms or matches the performance of existing arrays across all essential metrics. Typically, eight-element arrays function within the frequency range of 3.7–12.5 GHz, while this research employs only four elements at 7.5 GHz, thereby reducing complexity without compromising performance. Earlier four-element designs indicated return losses ranging from -16 dB to -30 dB and gains between 7.73 and 12 dBi, often neglecting to report efficiency figures. In contrast, the current array achieves a return loss of -49.1 dB, which is significantly lower than previous measurements. Its recorded gain of 14.1 dBi matches the highest result documented in [13]. The sidelobe level is reduced to -20 dB, surpassing the earlier designs. Importantly, the radiation efficiency reaches 94.4 percent, exceeding the 71.5 percent and 86.7 percent reported in the limited studies that included this metric. Overall, this four-element array provides excellent impedance matching, high gain, effective sidelobe suppression, and remarkable efficiency. The outcome is a compact, high-performance solution that achieves an optimal balance between simplicity and effectiveness for X-band satellite communications.

5. CONCLUSION

This work codesigned and validated an inclined microstrip patch array using a corporate feed and an ANN surrogate for 7.5 GHz meteorological direct broadcast. The fabricated 1×4 prototype on RT Duroid 5880 with $\varepsilon_r = 2.2$ and $h = 0.787$ mm achieved a 7.5 GHz center frequency, a 10 dB impedance bandwidth near 450 MHz, broadside patterns, and measured peak gain above 14 dBi. Extending the surrogate-driven workflow to 1×8, 1×16, 1×32, and 1×64 confirmed about 3 dB gain per doubling, progressive beamwidth narrowing, and stable bandwidth near 450 MHz, while alternate 45° rotation and rounded corners limited surface modes and mutual coupling. These results establish a compact and scalable path to high-gain X-band arrays for ground terminals. Future developments will integrate the ANN with Bayesian or reinforcement learning optimizers for automated multi-objective synthesis that controls S_{11}, coupling, amplitude, phase balance, sidelobe level, and tolerance robustness. Additional directions include dual-polarized and wide-scan subarrays, loss-aware corporate or substrate-integrated waveguide feeds, low-loss reconfigurable elements for electronic steering, aperiodic layouts for sidelobe reduction, and surrogates that include radome, thermal drift, rainfall, and aging, followed by system-level validation of gain over temperature and rain margin.

REFERENCES

[1] Haupt, R. L. and Y. Rahmat-Samii, "Antenna array developments: A perspective on the past, present and future," *IEEE Antennas and Propagation Magazine*, Vol. 57, No. 1, 86–96, 2015.

[2] Sun, J., "A novel design of 45° linearly polarized array antenna with taylor distribution," *Progress In Electromagnetics Research Letters*, Vol. 106, 151–155, 2022.

[3] Nguyen, D. H., J. Ala-Laurinaho, J. Moll, V. Krozer, and G. Zimmer, "Improved sidelobe-suppression microstrip patch antenna array by uniform feeding networks," *IEEE Transactions on Antennas and Propagation*, Vol. 68, No. 11, 7339–7347, 2020.

[4] Lu, Y., L. Zhou, M. Cui, X. Du, and Y. Hu, "A method for planar phased array calibration," *Progress In Electromagnetics Research Letters*, Vol. 94, 19–25, 2020.

[5] Yang, H., T. Li, L. Xu, X. Cao, J. Gao, J. Tian, H. Yang, and D. Sun, "A new strategy to design microstrip antenna array with low side-lobe level and high gain," *IEEE Access*, Vol. 7, 152 715–152 721, 2019.

[6] Tang, X.-R., S.-S. Zhong, Z. Sun, and J.-J. Liu, "Low-cost low-sidelobe microstrip array with circular polarization," *Microwave and Optical Technology Letters*, Vol. 50, No. 9, 2384–2386, 2008.

[7] Mohammadi Shirkolaei, M., H. R. D. Oskouei, and M. Abbasi, "Design of 1 * 4 microstrip antenna array on the human thigh with gain enhancement," *IETE Journal of Research*, Vol. 69, No. 9, 5944–5950, 2023.

[8] Tan, M. C., M. Li, Q. H. Abbasi, and M. A. Imran, "A wideband beamforming antenna array for 802.11 ac and 4.9 GHz in modern transportation market," *IEEE Transactions on Vehicular Technology*, Vol. 69, No. 3, 2659–2670, 2020.

[9] Sedgeechongaraluye-Yekan, T., R. A. Sadeghzadeh, and M. Naser-Moghadasi, "Microstrip-fed circularly polarized antenna array using semi-fractal cells for implicational band," *IETE Journal of Research*, Vol. 60, No. 6, 383–388, 2014.

[10] Miligy, A. F., F. Taher, M. F. A. Sree, S. Y. A. Fatah, T. Alghamdi, and M. Alathbah, "Investigation and implementation of miniaturized microwave system for linear array antenna loaded with omega structures planar array," *IEEE Access*, Vol. 12, 82 636–82 646, 2024.

[11] Pandhare, R. A., P. L. Zade, and M. P. Abegaonkar, "Miniaturized microstrip antenna array using defected ground structure with enhanced performance," *Engineering Science and Technology, an International Journal*, Vol. 19, No. 3, 1360–1367, 2016.

[12] Abushakra, F. Z., A. S. Al-Zoubi, and D. F. Hawatmeh, "Design and measurements of rectangular dielectric resonator antenna linear arrays," *Applied Computational Electromagnetics Society Journal (ACES)*, Vol. 33, No. 4, 380–387, 2018.

[13] Abishek, E., R. Subramaniam, P. Ramanujam, and M. Esakkimuthu, "Low-profile circularly polarized conformal antenna array with side lobe suppression for vehicular SATCOM applications," *Applied Computational Electromagnetics Society Journal (ACES)*, Vol. 38, No. 6, 439–447, 2023.

[14] Kola, K. S., A. Chatterjee, and D. Patanvariya, "Design of a compact high gain printed octagonal array of spiral-based fractal antennas for DBS application," *International Journal of Microwave and Wireless Technologies*, Vol. 12, No. 8, 769–781, 2020.

[15] Niu, Z., H. Zhang, Q. Chen, and T. Zhong, "A novel defect ground structure for decoupling closely spaced E-plane microstrip antenna array," *International Journal of Microwave and Wireless Technologies*, Vol. 11, No. 10, 1069–1074, 2019.

[16] Sameena, N. M., R. B. Konda, and S. N. Mulgi, "Broadband, high-gain complementary-symmetry microstrip array antenna," *Microwave and Optical Technology Letters*, Vol. 52, No. 10, 2256–2258, 2010.

[17] Patanvariya, D. G., A. Chatterjee, and K. S. Kola, "High-gain and circularly polarized fractal antenna array for dedicated short range communication systems," *Progress In Electromagnetics Research C*, Vol. 101, 133–146, 2020.

[18] Liu, F., Z. Zhang, W. Chen, Z. Feng, and M. F. Iskander, "An endfire beam-switchable antenna array used in vehicular environment," *IEEE Antennas and Wireless Propagation Letters*, Vol. 9, 195–198, 2010.

[19] Nikkhah, M. R., A. A. Kishk, and J. Rashed-Mohassel, "Wideband DRA array placed on array of slot windows," *IEEE Transactions on Antennas and Propagation*, Vol. 63, No. 12, 5382–5390, 2015.

[20] Garbaruk, M., "A planar four-element UWB antenna array with stripline feeding network," *Electronics*, Vol. 11, No. 3, 469, 2022.

[21] Al-Mumen, H. and A. A. Hamad, "Design and characterization of an radio frequency reused energy system for nano-devices," *Bulletin of Electrical Engineering and Informatics*, Vol. 11, No. 5, 2595–2602, 2022.

[22] Hasan, M. F., D. A. A. Mat, and M. A. Sayed, "Modified backline inset feed 1 × 4 array microstrip antenna for 5.8 GHz frequency band," *Indonesian Journal of Electrical Engineering and Computer Science (IJEECS)*, Vol. 36, No. 2, 892–900, 2024.

[23] Arce, A., F. Arce, E. Stevens-Navarro, U. Pineda-Rico, M. Cardenas-Juarez, and A. Garcia-Barrientos, "Recurrent deep learning for beam pattern synthesis in optimized antenna arrays," *Applied Sciences*, Vol. 15, No. 1, 204, 2025.

[24] Belen, M. A., A. Caliskan, S. Koziel, A. Pietrenko-Dabrowska, and P. Mahouti, "Optimal design of transmitarray antennas via low-cost surrogate modelling," *Scientific Reports*, Vol. 13, No. 1, 15044, 2023.

[25] Montaser, A. M. and K. R. Mahmoud, "Deep learning based antenna design and beam-steering capabilities for millimeter-wave applications," *IEEE Access*, Vol. 9, 145 583–145 591, 2021.

[26] Pratigya, M. and G. Kumar, "Antenna at S-band as ground for array at X-band in dual frequency antenna at S/X-bands," *Progress In Electromagnetics Research Letters*, Vol. 71, 15–22, 2017.

[27] Toso, G., C. Mangenot, and A. G. Roederer, "Sparse and thinned arrays for multiple beam satellite applications," in *2nd European Conference on Antennas and Propagation (EuCAP 2007)*, 1–4, Edinburgh, 2007.